AGU PUBLICATIONS

JGR

Journal of Geophysical Research: Atmospheres

RESEARCH ARTICLE
10.1002/2015JD023622

Key Points:
- Stratospheric water vapor in monsoons controlled by subtropical dehydration
- Enhanced tropospheric convection leads to reduced stratospheric water vapor
- Overshooting convection is not dominant process for stratospheric water vapor in monsoons

Correspondence to:
W. J. Randel,
randel@ucar.edu

Citation:
Randel, W. J., K. Zhang, and R. Fu (2015), What controls stratospheric water vapor in the NH summer monsoon regions?, *J. Geophys. Res. Atmos.*, *120*, 7988–8001, doi:10.1002/2015JD023622.

Received 1 MAY 2015
Accepted 17 JUL 2015
Accepted article online 20 JUL 2015
Published online 10 AUG 2015

©2015. American Geophysical Union. All Rights Reserved.

What controls stratospheric water vapor in the NH summer monsoon regions?

William J. Randel[1], Kai Zhang[2], and Rong Fu[2]

[1]National Center for Atmospheric Research, Boulder, Colorado, USA, [2]Department of Geological Sciences, University of Texas, Austin, Texas, USA

Abstract Water vapor in the lower stratosphere exhibits localized maximum values during Northern Hemisphere summer in the Asian and North American (NA) monsoon regions. The processes maintaining these maxima are not well understood. We analyze the variability of water vapor in the monsoon regions based on Aura Microwave Limb Sounder satellite observations during 2005–2013 and quantify links to deep convection, large-scale temperatures, and monsoonal circulations. Strong subseasonal variations in stratospheric water vapor are closely linked with deep convection in the monsoon regions, with the surprising result that stronger convection leads to a relatively dry stratosphere and weaker convection to a wetter stratosphere. This result is observed for both the Asian and NA monsoon regions. This behavior is explained by temperature changes in the stratosphere tied to deep convection: stronger convection leads to relatively cold temperatures in the subtropical lower stratosphere, which is the key region controlling large-scale dehydration within the anticyclonic monsoonal circulations. Likewise, weaker convection leads to warmer subtropical stratospheric temperatures, relatively less dehydration, and enhanced water vapor. The observed water vapor changes are in approximate agreement with those expected from the subtropical temperature variations, taking into account dilution of the dehydrated air into the larger monsoon region. These results demonstrate that stratospheric water vapor in the Northern Hemisphere monsoon regions is mainly controlled by large-scale circulation and temperatures, and overshooting deep convection plays a relatively minor role.

1. Introduction

Satellite observations indicate that water vapor in the lower stratosphere (LS) is characterized by localized maxima during the Northern Hemisphere (NH) summer in the regions of the Asian and North American (NA) monsoons [*Rosenlof et al*., 1997; *Randel et al*., 2001; *Dessler and Sherwood*, 2004; *Milz et al*., 2005; *Park et al*., 2007]. These climatological summertime maxima can influence much of the NH via large-scale transport [*Ploeger et al*., 2013] and contribute to the moist phase of the annual cycle in global stratospheric water vapor. The LS water vapor maxima occur near regions of deep convection and are embedded within anticyclonic circulations that characterize the upper troposphere/lower stratosphere (UTLS) monsoon regions. While the climatological behaviors of the LS water vapor maxima are well known, the processes that maintain and control this behavior are less well understood. In particular, the relative influences of overshooting deep convection and large-scale circulation and in situ dehydration are poorly known. This study examines the variability of water vapor in the monsoon regions from satellite measurements, in conjunction with observed deep convection and circulation/temperature behavior, to improve understanding of the processes influencing observed variability.

There are observational and modeling results that suggest the importance of both overshooting deep convection and large-scale processes for the LS summer monsoon regions. Aircraft measurements have shown evidence of strong LS water vapor enhancements in the NA region during summer [e.g., *Ray et al*., 2004; *Hanisco et al*., 2007; *Anderson et al*., 2012]. *Fu et al*. [2006] suggested an important role for convective transport to the stratosphere over the Tibetan Plateau, and the behavior of deep convection reaching altitudes near the tropopause in the Asian monsoon has been analyzed by *Devasthale and Fueglistaler* [2010]. *Wang* [2003] provided high-resolution simulations of convective plumes transporting water vapor to the lower stratosphere over NA during summertime. Infrequent cases of enhanced LS water vapor over both Asian and NA summer monsoon regions, providing evidence of convective overshooting, have been documented in satellite measurements by *Schwartz et al*. [2013]. Furthermore, observations of enhanced water vapor isotopic ratios (HDO/H_2O) in the monsoon regions [*Hanisco et al*., 2007; *Randel et al*., 2012]

support a role for overshooting deep convection. On the other hand, model calculations based on large-scale circulation and temperature fields (without the effects of explicit or parameterized overshooting convection) can reproduce many aspects of LS water vapor in the monsoon regions, including seasonal and spatial structures and approximate correct magnitudes. Such models include full general circulation models [*Bannister et al*., 2004; *Gettelman et al*., 2004] and Lagrangian trajectory models [*James et al*., 2008; *Wright et al*., 2011; *Schoeberl et al*., 2013]. The Lagrangian calculations of *James et al*. [2008] and *Wright et al*. [2011] both utilize satellite cloud measurements to determine where trajectories are hydrated by deep convection, while *Schoeberl et al*. [2013] do not include this mechanism. The global models also suggest the importance of monsoons for transport to the tropics and global stratosphere [*Dethof et al*., 1999; *Bannister et al*., 2004; *Gettelman et al*., 2004; *Ploeger et al*., 2013].

In this study we examine the variability of LS water vapor in the monsoon regions based on 9 years of daily satellite observations, and quantify links with fluctuations in deep convection (using outgoing longwave radiation, OLR) and large-scale circulation and temperature, based on meteorological reanalyses. Our objective is to use the natural (subseasonal) variability of the monsoon systems to identify physical links that contribute to maintaining overall balances.

2. Data and Analyses

2.1. Microwave Limb Sounder Water Vapor

Our analyses are based on satellite water vapor measurements from the Aura Microwave Limb Sounder (MLS), obtained from MLS version 3.3 level 2 products (http://mls.jpl.nasa.gov/products/h2o_product.php). The MLS instrument aboard the Aura spacecraft has been providing simultaneous global measurements of various chemical species including water vapor in the lower and middle atmosphere since August 2004, and our analyses cover the NH summer seasons from 2005 to 2013. We constructed gridded daily data by averaging profiles inside bins with resolution of 5° latitude × 10° longitude. We processed individual profiles following the instructions in *Livesey et al*. [2011]. The typical single-profile precisions for water vapor are 0.9, 0.7, 0.5, and 0.3 ppmv at 215, 147, and 100 hPa and lower stratosphere, respectively [*Livesey et al*., 2011].

2.2. OLR and ERA-Interim Meteorological Analyses

NOAA-interpolated outgoing longwave radiation (OLR) data are used as a proxy for deep convection, with daily gridded analyses obtained from NOAA-Cooperative Institute for Research in Environmental Sciences Climate Diagnosis Center (http://www.cdc.noaa.gov/). The horizontal resolution is 2.5° × 2.5°. We also use daily meteorological analyses from ERA-Interim reanalysis [*Dee et al*., 2011], including temperature and wind fields, and diabatic heating extracted from the reanalysis archive (diabatic heating rates are output from the reanalysis model forecast fields). The horizontal resolution for these data is 1.5° × 1.5°. For all the parameters, we utilize data overlapping the period of MLS water vapor observations.

2.3. Statistical Significance for Composite Calculations

Our analyses are based upon compositing OLR and circulation statistics for wet and dry anomalies of LS water vapor during the summers of 2005–2013. We evaluate the statistical significance of the composited results by comparison to statistics derived from resampling the original data in a random manner. Specifically, composite statistics are derived from 10,000 random samples of the original data, and significance levels for the actual composites are evaluated compared to the 95% level of the randomly sampled data.

3. Results

3.1. Climatological Behavior

The climatological monthly evolution of water vapor at 100 hPa during May–August is shown in Figure 1, based on MLS data during 2005–2013. Isolated maxima are observed over the Asian and NA monsoon regions throughout the summer (June–August); the Asian maximum develops slightly earlier (May) than that over NA. Lower stratosphere water vapor increases throughout the summer on a broad scale, and persists over northern midlatitudes into autumn (November), but without clear localized maxima over the monsoon regions beyond August. This global-scale behavior primarily follows the strong annual cycle of dehydration in the deep tropics [e.g., *Schoeberl and Dessler*, 2011].

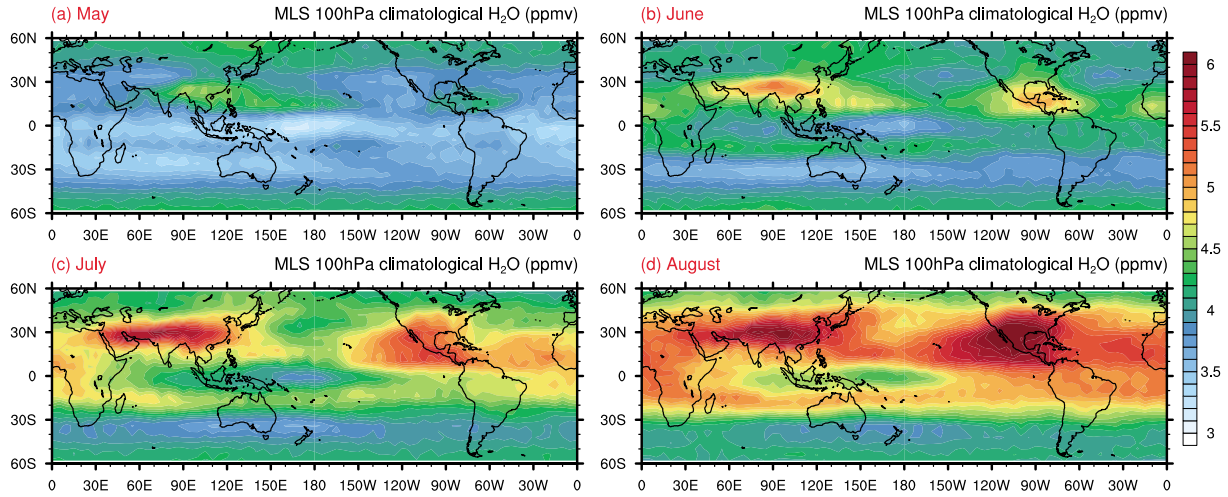

Figure 1. (a–d) Climatological monthly mean water vapor at 100 hPa during May to August, derived from MLS measurements during 2005–2013.

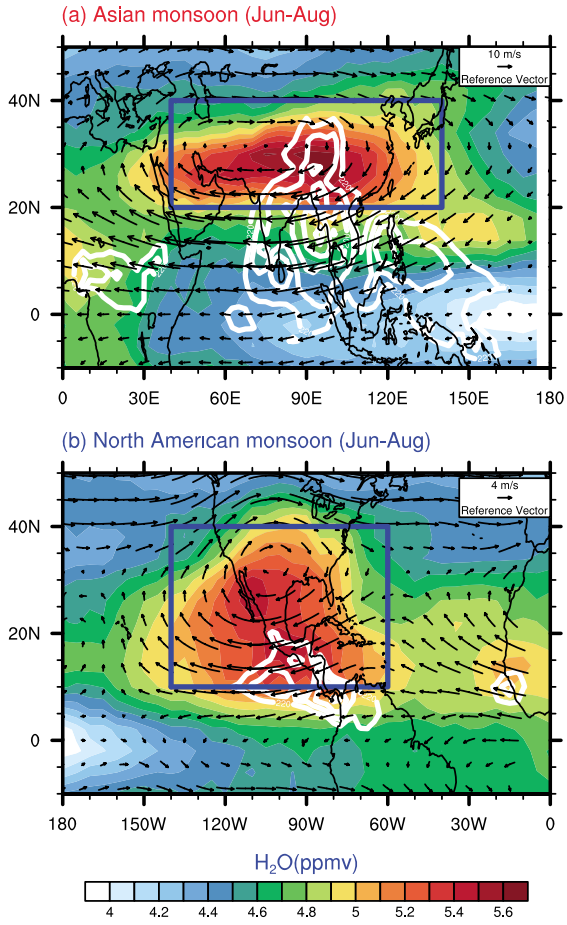

Figure 2. The colors show the climatological structure of water vapor during summer (June–August) for the (a) Asian and (b) NA monsoon regions, together with the time average circulation (horizontal winds at 100 hPa) and deep convection (OLR in white lines). The blue boxes outline the domains over which time series of water vapor are calculated.

The climatological behavior of water vapor and circulation at 100 hPa for both monsoon regions are shown in Figure 2 for averages during June–August, together with the corresponding patterns of deep convection (OLR). As is well known, the UTLS circulation in both monsoon regions is dominated by anticyclonic flow, centered to the northwest of the main convective regions [e.g., *Hoskins and Rodwell*, 1995; *Park et al.*, 2007]. The anticyclonic circulation in the Asian monsoon is substantially stronger than that over NA, as is the corresponding diabatic heating diagnosed from meteorological data [*Hoskins and Rodwell*, 1995]. In both monsoon regions, the area of relatively high lower stratospheric water vapor is not centered above the deep convection but is more closely aligned with the anticyclonic circulation. Regarding the influence of overshooting deep convection, it is relevant to note that MLS data [*Schwartz et al.*, 2013] show extreme water vapor values (indicative of convection penetrating into the lower stratosphere) approximately coaligned with the climatological maxima over Asia in Figure 2a. In contrast, the patterns of extreme water vapor over NA occur primarily over the United States, on the northern edge of the broad-scale pattern seen in Figure 2b.

One aspect of the Asian monsoon trajectory model calculations of *Wright et al.* [2011] of relevance to our study is that dehydration primarily occurs on the equatorward (cold) side of the lower stratospheric anticyclonic circulation [*Wright et al.*, 2011, their Figure 4]. A similar situation probably occurs over the NA monsoon,

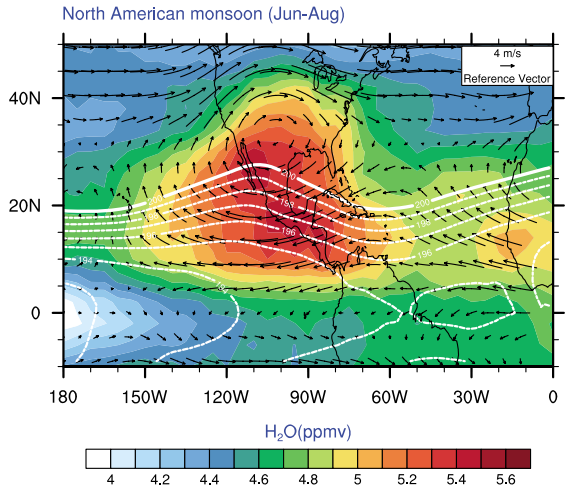

Figure 3. Climatological water vapor and circulation for the NA monsoon (as in Figure 2), with the superimposed white contours showing the background 100 hPa temperature structure (with contours only for temperature less than 200 K).

where the coldest temperatures also occur on the equatorward side (Figure 3). The importance of flow through the cold region of the monsoons is analogous to the controlling influence of the (cold) western Pacific on tropical stratospheric water vapor highlighted by *Holton and Gettelman* [2001].

3.2. Water Vapor Variability in the Monsoon Regions

Our analysis focuses on the daily variability of 100 hPa water vapor in the monsoon regions during summer for the years 2005–2013. While the isolated monsoon maxima are most evident for the months of June–August, our statistical analysis uses data during May–September to include variability at either end of the summer (results are very similar using only the June–August period). We calculate monsoon regional averages for each day over the domains 20–40°N, 40–140°E and 10–40°N, 60–140°W, for the Asian and NA monsoons, respectively; these regions are noted in Figure 2. In each region we subtract a smoothly varying seasonal cycle to derive deseasonalized anomalies for each year, as shown in Figures 4a and 4b (with the 9 years plotted together as a nearly continuous time series). These time series show some substantial year-to-year variability superimposed on faster subseasonal maxima. In order to focus on the subseasonal variability and associated links with convection, temperatures, and circulation, we aim to remove components of the interannual variability. However, relatively little is known about the interannual variability of stratospheric water vapor in the monsoon regions. Based on previous work showing links between stratospheric water vapor and the quasi-biennial

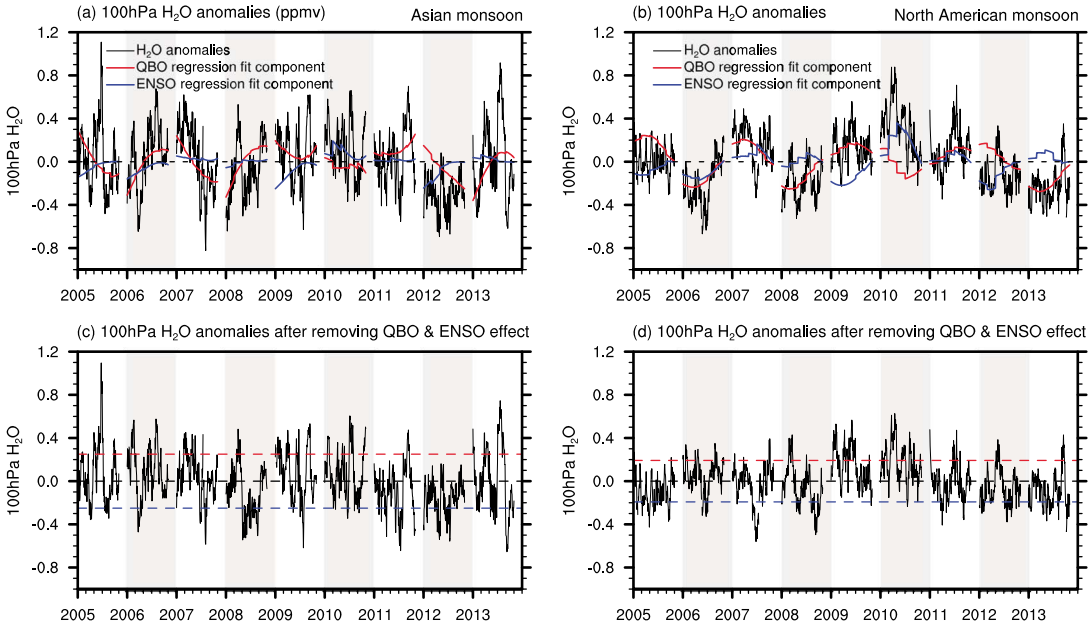

Figure 4. Time series of deseasonalized 100 hPa water vapor anomalies in the (a and c) Asian and (b and d) NA monsoon regions. Time series show data for May–September of each year 2005 to 2013, with each tick representing 1 month. Figures 4a and 4b show full anomalies, together with regression fits to the QBO (red lines) and ENSO variability (blue lines); the color curves are not continuous because only the summertime part of the time series is shown. Figures 4c and 4d show the water vapor anomalies with the QBO and ENSO fits removed to highlight subseasonal variability. The dashed lines in Figures 4c and 4d are at 1 sigma variability and are used to identify extreme wet and dry anomalies.

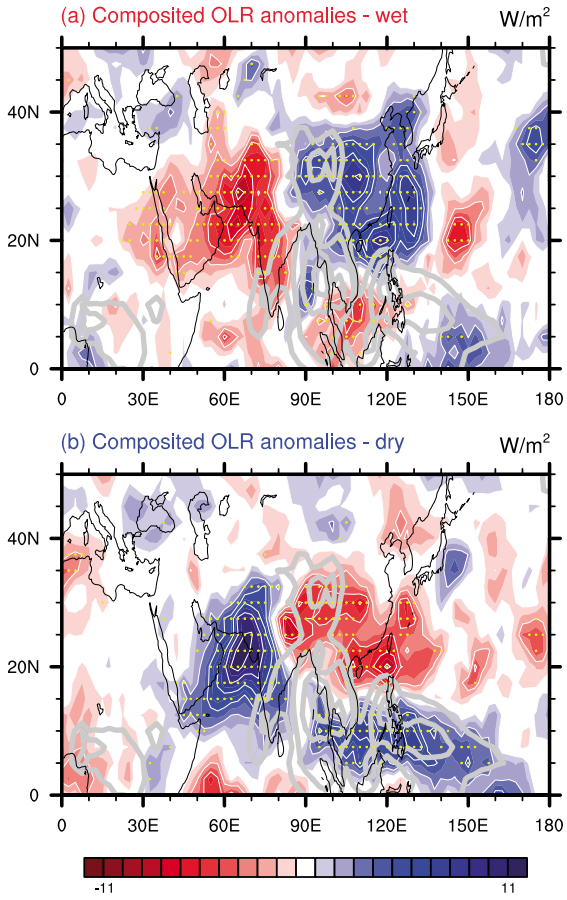

Figure 5. Composited OLR anomalies for (a) wet and (b) dry stratospheric water vapor extrema over the Asian monsoon region. Results are shown for OLR averaged 0–10 days prior to the stratospheric water vapor extrema. The colors indicate the OLR variations, with red (low OLR) denoting enhanced deep convection. Stippling denotes the regions of statistical significance. The grey lines indicate the background average OLR, highlighting the location of climatological deep convection.

oscillation (QBO) [e.g., *Giorgetta and Bengtsson*, 1999; *Geller et al.*, 2002] and with the El Niño–Southern Oscillation (ENSO) [e.g., *Gettelman et al.*, 2001; *Fueglistaler and Haynes*, 2005], we fit the deseasonalized time series in Figures 4a and 4b with a multivariate linear regression based on standard QBO and ENSO proxies [e.g., *Randel et al.*, 2009]. The resulting fits are shown in Figures 4a and 4b, and capture much of the interannual variability, although these are simply empirical fits, and detailed mechanisms for QBO or ENSO influence on water vapor in the monsoon regions are not well understood (and note that the QBO and ENSO fits in Figure 4 are different for Asia and NA). Improved understanding of interannual variations in the monsoon regions may be a fruitful topic for future research.

The water vapor time series with the QBO and ENSO fits removed (Figures 4c and 4d) provide the basis for the remainder of this work. We composite OLR, temperature, and circulation statistics according to the wet and dry extremes, namely, values above and below 1 sigma standard deviation (dashed lines in Figures 4c and 4d). As described above, we test the significance of the results using resampling techniques. We note that there is somewhat larger variability of the water vapor anomalies over Asia (standard deviation $\sigma = 0.25$ ppmv) compared to NA ($\sigma = 0.19$ ppmv), possibly related to the overall stronger intensity of convection and/or more confined circulation over the Asian monsoon (e.g., Figure 2). Spatial patterns of the composited wet and dry monsoon anomalies (not shown here) reveal broad patterns that overlap the time-averaged structures shown in Figure 2, and we do not find distinctive spatial structures for the averages of either extreme.

While our focus is on the variability of monsoon water vapor at 100 hPa, we have also examined corresponding variability at higher levels. Fluctuations at 82 hPa nearly mirror those at 100 hPa, with approximately one half of the amplitude; correlations of subseasonal variations between 100 hPa and 82 hPa are 0.77 and 0.68 for the Asian and NA monsoon regions, respectively. For the Asian monsoon the variability at 68 hPa is reduced further but is still correlated with 100 hPa. The NA monsoon is no longer evident as an isolated water vapor maximum at and above 68 hPa, and likewise the Asian monsoon maximum disappears above 68 hPa. We note that these results are based on the relatively thick (~3 km) layers measured by MLS, with likely significant overlap of information between adjacent levels.

One further note regards the analysis of water vapor on isentropes versus pressure levels. The relatively fast circulation in the monsoon regions might suggest that our analyses should be focused on isentropic levels versus pressure levels native to the MLS retrievals. However, this has the disadvantage of requiring interpolation of all data to isentropic levels, with attendant uncertainties (especially regarding the thick layer MLS data). Moreover, we have tested such calculations and find nearly identical variability for water vapor diagnosed on the 400 K isentrope compared to 100 hPa (Figure 4). Accordingly, we choose to perform our analyses based on pressure levels.

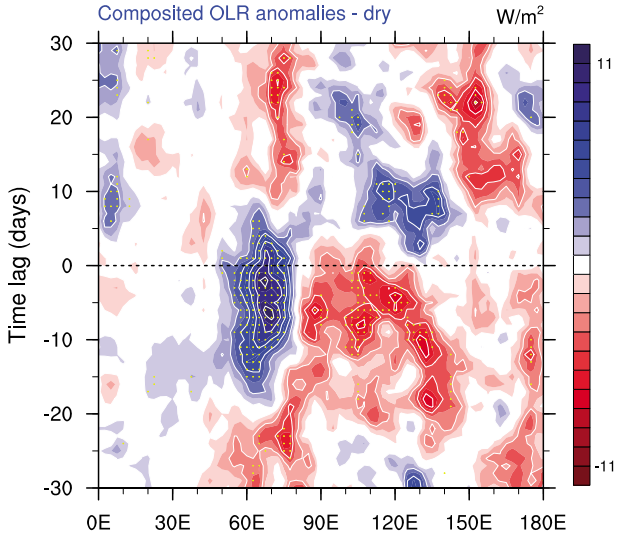

Figure 6. Time variations of OLR anomalies over 20–30°N composited for dry stratospheric water vapor extremes in the Asian monsoon region. Red indicates enhanced deep convection, and stippling denotes statistically significant results.

3.3. Asian Monsoon

OLR anomalies composited for the wet and dry stratospheric H_2O anomalies over the Asian monsoon are shown in Figure 5. The overall patterns show an east-west dipole structure to the OLR anomalies in both cases, with high statistical coherence with the stratospheric H_2O variations. The east-west dipole patterns are a signature of longitudinal shifts in the large-scale deep convection. Comparisons with the background OLR structure (grey contours in Figures 5a and 5b) show that the anomalous OLR variations over the eastern portion of the dipole act to reinforce or decrease the strongest climatological deep convection near ~80–110°E; the sign of the anomalies is such that stronger deep convection occurs in association with a relatively dry stratosphere (Figure 5b) and weaker convection for a wet stratosphere (Figure 5a). While the anomalies on the western side of the dipole (~50–80°E) are as strong as on the eastern side, they probably have little direct influence (via overshooting convection) on the lower stratosphere, as they occur in a region of weaker climatological deep convection.

Temporal variations of the dry stratosphere composited OLR anomalies over 20–30°N (near the center of the patterns in Figure 5b) are shown in Figure 6 (i.e., the composited OLR leads or lags the stratospheric water vapor). Enhanced convection over ~80–140°E precedes the stratospheric dry anomalies by ~0–10 days, consistent with a causal link; during this time, decreases in convection occur over ~50–80°E. Temporal variations in Figure 6 suggest oscillation time scales for the large-scale convection of ~30–50 days, which is consistent with previous analyses of low-frequency variations in the Asian monsoon circulation statistics [e.g., *Yasunari*, 1981; *Lau and Chan*, 1986; *Annamalai and Slingo*, 2001].

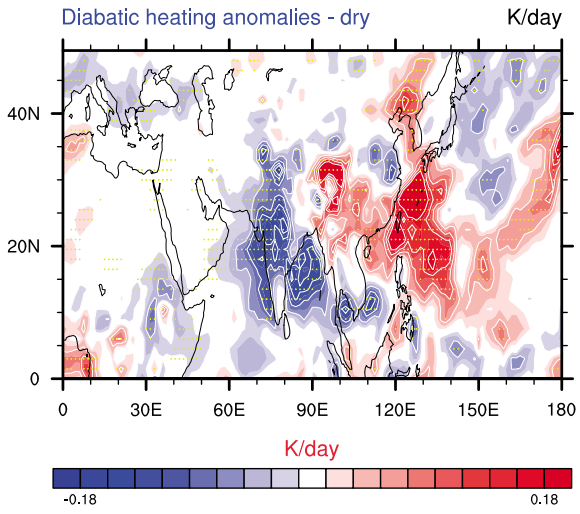

Figure 7. Composited anomalies in tropospheric column average (700–200 hPa) diabatic heating (K/d) for dry stratospheric water vapor extrema over the Asian monsoon. Results are shown for diabatic heating 0–10 days prior to the stratospheric water vapor anomaly minimum.

As discussed in the Introduction, variations in deep convection can influence LS water vapor via direct overshooting and by modifying large-scale circulation and temperatures. In the latter case, the causal mechanism is related to changes in diabatic heating linked to the convection (and note that the large-scale diabatic heating is responsible for the presence of the summer monsoon UTLS anticyclonic circulations in the first place [e.g., *Hoskins and Rodwell*, 1995]). We have examined the diabatic heating estimates obtained from the ERA-Interim reanalysis and find strong correlations with observed variations in OLR. For example, Figure 7 shows diabatic heating anomalies (averaged in the vertical over 700–200 hPa) composited for dry stratospheric water vapor anomalies, showing a clear east-west dipole structure that is highly correlated with the composited OLR patterns in Figure 5b, indicating that enhanced convection is linked with stronger diabatic heating (and vice versa).

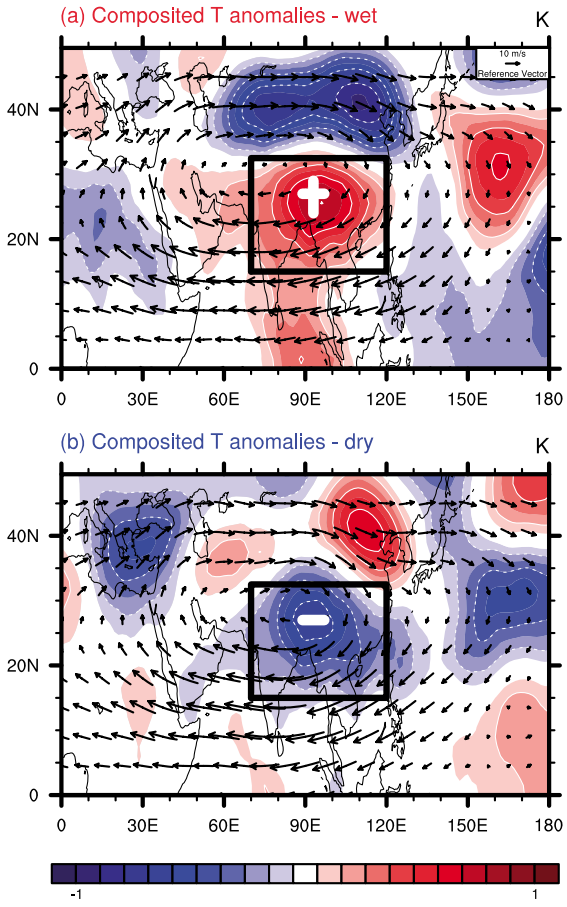

Figure 8. Composited temperature anomalies at 100 hPa for (a) wet and (b) dry stratospheric water vapor extrema over the Asian monsoon region. Results are shown for temperatures averaged 0–10 days prior to the water vapor anomaly extrema. The plus and minus signs highlight the subtropical regions which influence dehydration in the stratosphere. The wind vectors indicate the climatological anticyclonic circulation at 100 hPa.

While this behavior is expected, these results confirm a physical link between diabatic heating linked to deep convection and large-scale circulations in the monsoon regions. Similar coherence between OLR and diabatic heating is found for wet and dry LS water vapor composites for both Asian and NA monsoon regions (results not shown).

A key link between the large-scale circulation and stratospheric water vapor is temperature in the lower stratosphere, and Figure 8 shows temperatures at 100 hPa composited for the Asian monsoon stratospheric H_2O extremes. The temperature patterns show north-south dipole patterns centered on the climatological anticyclone (indicated by the circulation vectors in Figure 8). The sign of the temperature anomalies is such that a wet stratosphere is linked to warm temperatures on the south side of the anticyclone (Figure 8a) and vice versa for the dry stratosphere (Figure 8b). This is precisely the behavior expected from the calculations of *Wright et al.* [2011], who highlight the importance of dehydration on the south (cold) side of the anticyclone for controlling stratospheric water vapor.

Further aspects of the three-dimensional temperature and wind variations of the Asian monsoon associated with stratospheric water vapor extremes are shown in the latitude-height cross sections in Figure 9 (through the center of the anticyclone, averaged over 70–120°E). Temperature anomalies are evident in the lower stratosphere (consistent with Figure 8), and there are furthermore out-of-phase patterns in the troposphere so that the temperatures exhibit an overall quadrupole structure. There are corresponding maxima in zonal wind anomalies in the UTLS (in thermal wind balance with the temperatures), which reflects variations in the intensity of the anticyclonic circulation, and these variations are approximately in phase or out of phase with the climatological anticyclone structure in Figure 2a. Stratospheric dry anomalies (Figure 9b) are linked with a stronger anticyclone and a warm troposphere and cold lower stratosphere over ~15–30°N (and oppositely signed temperatures north of 35°N). These dynamical variations are tied to enhanced deep convection (Figure 5b) and diabatic heating (Figure 7) east of 80°E. Nearly opposite patterns are seen for the wet stratosphere composites (Figure 9a): colder subtropical troposphere, warmer lower stratosphere, and weaker anticyclone (coupled with weaker convection; Figure 5a). The overall circulation exhibits balanced dynamical structure (as expected), while it is the temperatures in the subtropical lower stratosphere that are of most direct relevance for the LS monsoon water vapor.

Figure 10 illustrates the temporal variations in key quantities during one individual summer (2009) that highlight the links shown in the composites. During this summer there are several distinct maxima in LS water vapor (±0.4 ppmv), with an approximate 30–40 day time scale (top curve in Figure 10). Figure 10 shows that these H_2O changes are simply linked to 100 hPa temperatures in the subtropics and to changes in tropospheric deep convection (less convection, warmer subtropical temperatures, and enhanced water vapor, with OLR and temperatures slightly preceding H_2O).

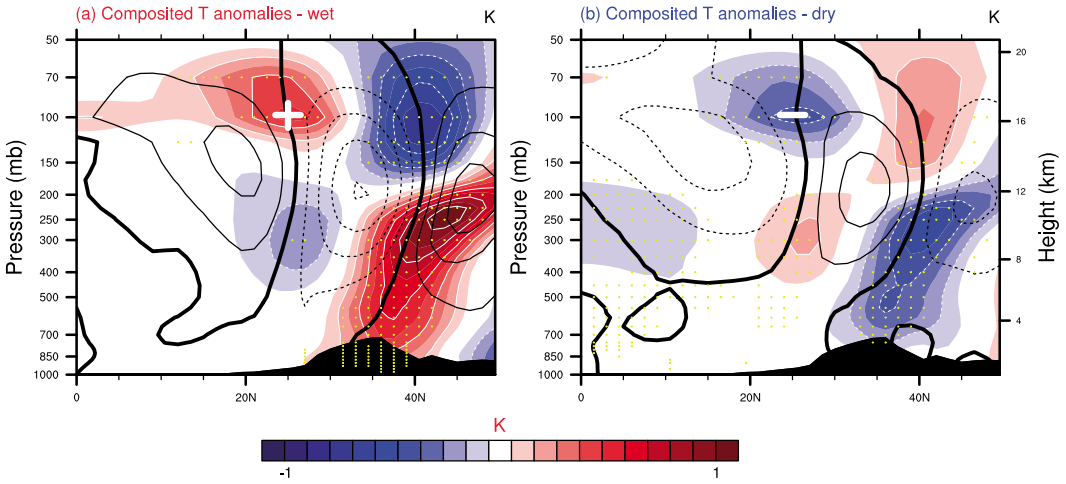

Figure 9. Latitude-height cross sections of composited temperature (colors) and zonal wind anomalies (contours, with contour interval of 1 m/s) averaged over 70–120°E for (a) wet and (b) dry stratospheric water vapor extremes over the Asian monsoon region. The solid (dashed) contours indicate the westerly (easterly) wind anomalies. Results are shown for temperatures and winds averaged 0–10 days prior to the water vapor anomaly extrema. The white plus and minus signs highlight the temperature anomalies in the subtropical stratosphere which primarily influence stratospheric water vapor.

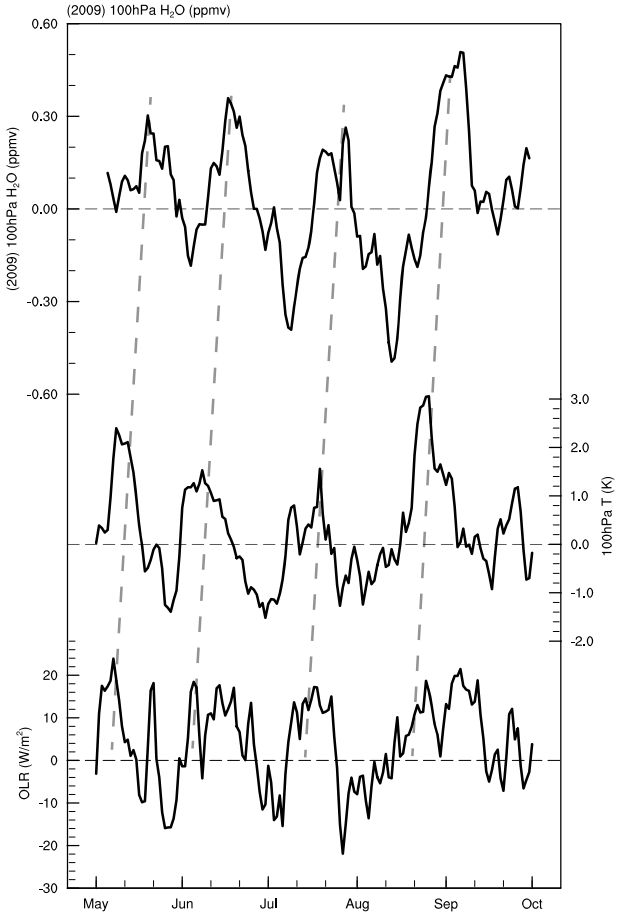

Figure 10. Time series of key variations in the Asian monsoon region during May–September 2009. Results show (top) 100 hPa water vapor anomalies in the monsoon region, (middle) 100 hPa temperature anomalies in the subtropics, and (bottom) OLR anomalies in the key convective region identified in Figure 5 (20–30°N, 90–120°E). Positive OLR anomalies indicate reduced deep convection.

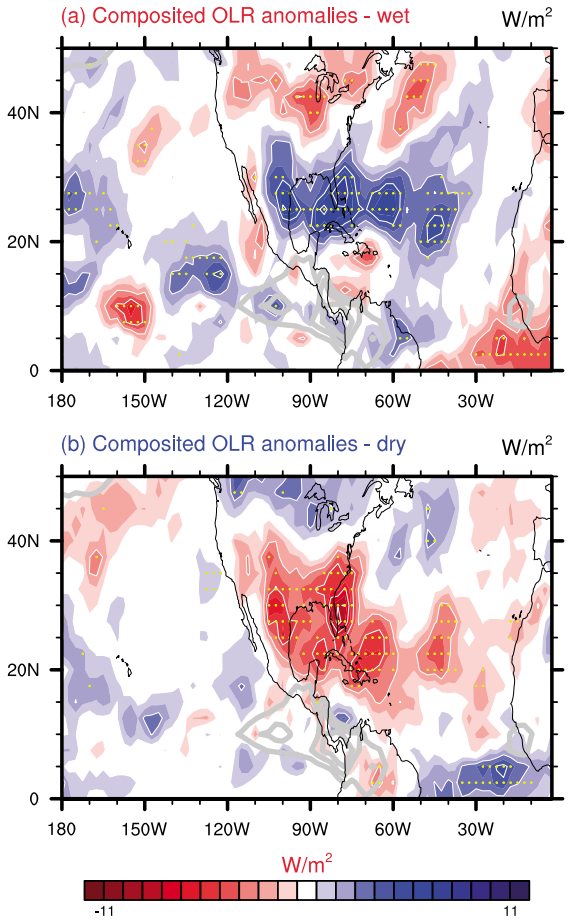

Figure 11. Composited OLR anomalies for (a) wet and (b) dry stratospheric water vapor extrema over the NA monsoon region. Results are shown for OLR averaged 0–10 days prior to the stratospheric water vapor anomaly extrema. The red colors (low OLR) denote enhanced deep convection. Stippling denotes regions of statistical significance. The grey lines indicate the background climatological deep convection.

3.4. NA Monsoon

OLR anomalies composited for extreme wet and dry stratospheric anomalies above the NA monsoon are shown in Figure 11. Strongly significant OLR variations are seen in both composites, centered over the southern United States and Gulf of Mexico (~20–35°N) and extending over the western Atlantic Ocean, and the sign of the composites is such that stronger convection is linked with a relatively dry stratosphere (Figure 11b) and vice versa (Figure 11a). Note that the OLR variations in Figure 11 are substantially north of the time-mean climatological OLR maxima, which are centered over Central America. Variations of the OLR for the dry stratosphere composites are shown as a function of time lag in Figure 12, showing that enhanced convection precedes the dry stratosphere events by ~0–10 days (similar to the Asian monsoon results in Figure 6). A very similar, oppositely signed signature is found for the wet composites (not shown). There is less evidence of 30–40 day oscillatory behavior in the NA convection in Figure 12 compared to statistics for the Asian monsoon (Figure 6).

The 100 hPa temperature composites for the NA monsoon are shown in Figure 13. Patterns exhibit a north-south dipole structure centered near the anticyclonic circulation, with warm anomalies on the south side for the wet composites and cold anomalies for the dry composites. In both cases, there are somewhat stronger temperature anomalies on the north side, but these may have less relevance for stratospheric H_2O,

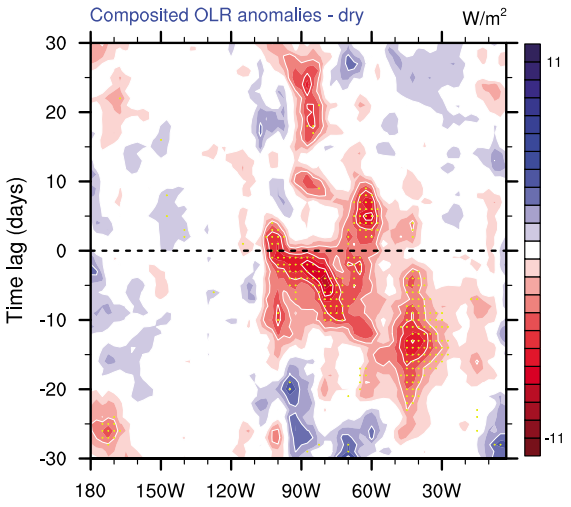

Figure 12. Time variations of OLR anomalies over 25–35°N composited for dry stratospheric water vapor extremes in the NA monsoon region. Red indicates enhanced deep convection, and stippling indicates statistically significant results.

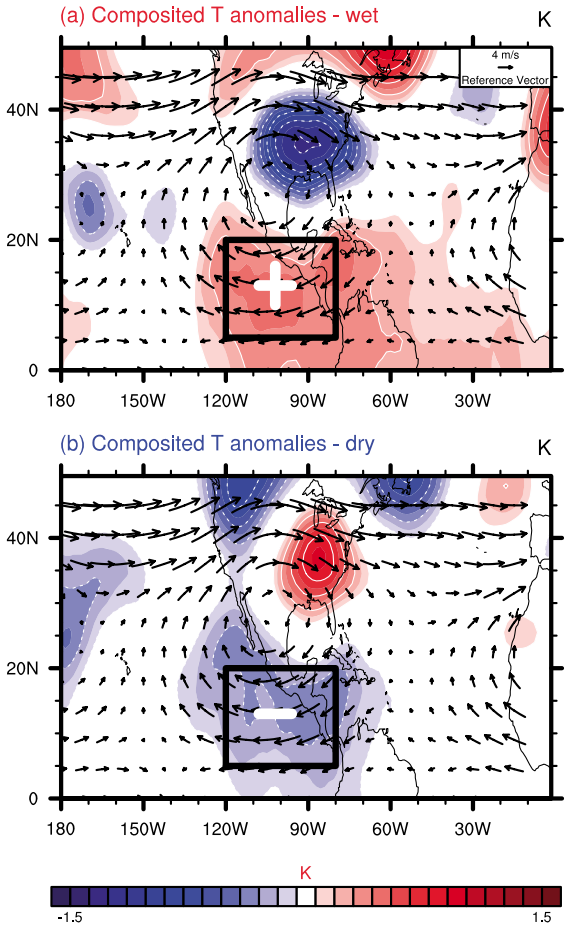

Figure 13. Composited temperature anomalies at 100 hPa for (a) wet and (b) dry stratospheric water vapor extrema over the NA monsoon region. Results are shown for temperatures averaged 0–10 days prior to the water vapor anomaly extrema. The plus and minus signs highlight the subtropical regions which influence dehydration in the stratosphere. The wind vectors indicate the climatological anticyclonic circulation at 100 hPa.

as dehydration will occur primarily on the climatologically colder south side, e.g., Figure 3.

Meridional cross-section composites for the zonal winds and temperatures (Figure 14) highlight lower stratospheric temperature anomalies with out-of-phase patterns in the troposphere, with the strongest anomalies over ~30–40°N. There are strong modulations of UTLS anticyclonic circulation in balance with the temperatures, although the patterns are centered on the temperature anomalies over 30–40°N, somewhat north of the climatological anticyclone shown in Figure 2b. The overall sense of the OLR, temperature, and circulation patterns is that a relatively wet LS is linked with reduced deep convection over 25–35°N (Figure 11a), warm temperatures in the subtropical lower stratosphere and northward displaced anticyclonic circulation; mirror images of these structures are found for the dry stratospheric composites.

3.5. Quantifying Water Vapor Versus Temperature Relationships

Our composite results suggest that temperatures in the subtropical lower stratosphere are the key factor controlling extreme variations in LS monsoon water vapor, via dehydration in the cold region of the anticyclone. These temperature variations are in turn forced by large-scale fluctuations in deep convection and diabatic heating in the troposphere. If subtropical temperatures are controlling stratospheric water vapor in the wider monsoon regions, then we anticipate that the water vapor anomalies will be linked to the subtropical temperatures via the Clausius-Clapeyron relationship. This behavior is tested for the Asian monsoon in Figure 15a, showing a two-dimensional distribution of the H_2O anomalies (in the wider monsoon region, i.e., the data in Figure 4c) versus temperatures in the subtropical LS (over the region of maximum temperature anomalies in Figure 8, 15–30°N and 70–120°E; boxed regions in Figure 8) for all June–August days during 2005–2013. Figure 15a also shows the functional relationship expected according to the dehydration at 100% relative humidity according to the Clausius-Clapeyron relationship (solid line), the latter expressed as anomalies from a reference at $T = 192$ K and 100 hPa. The results in Figure 15a show a significant correlation between H_2O and temperature ($r = 0.46$) but rather poor agreement with the theoretical curve.

Somewhat better agreement with theory can be obtained by assuming that the air is dehydrated in the subtropical temperature anomaly region and then diluted into the wider monsoon region. In the highly idealized situation where dehydration occurs in the (smaller) subtropical edge of the anticyclone and is diluted into the (larger) monsoon region, we can approximate the theoretically expected water vapor anomaly as that calculated according to the Clausius-Clapeyron relationship, scaled by the fractional area of the dehydration region compared to the larger monsoon. In the case of the Asian monsoon this fraction (i.e., the ratio of the boxed area in Figure 8 to the larger monsoon region in Figure 2a) is approximately one fourth. Figure 15a shows the results of this "diluted" calculation for a series of fractional areas (1/3, 1/5, and 1/7), showing that such dilution leads to a smaller H_2O versus temperature slope (as expected), with

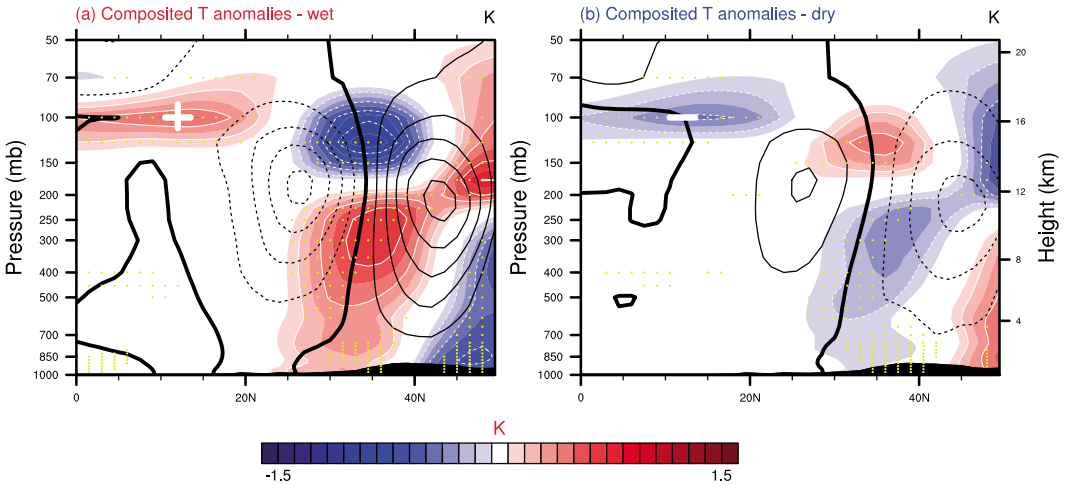

Figure 14. Latitude-height cross sections of composited temperature (colors) and zonal winds (contours, with contour interval of 1 m/s) averaged over 80–120°W for (a) wet and (b) dry stratospheric water vapor extremes over the NA monsoon region. Results are shown for temperatures and winds averaged 0–10 days prior to the water vapor anomaly extrema. The white plus and minus signs highlight the temperature anomalies in the subtropical stratosphere which primarily influence stratospheric water vapor.

results showing better agreement with the observed H2O versus temperature behavior. Although based on highly idealized assumptions, these calculations demonstrate that dehydration in the subtropics is a quantitatively reasonable model for understanding LS water vapor in the Asian summer monsoon.

Similar statistics and calculations are shown for the NA monsoon region in Figure 15b. In this case there is less variability in water vapor and weaker overall correlations with temperature ($r = 0.34$), although this is still a statistically significant relationship. Comparison with the (undiluted) Clausius-Clapeyron calculation (calculated for a reference $T = 195$ and 100 hPa; solid line in Figure 15b) shows poor agreement with the slope of the observed behavior. Considering dilution of the dehydrated air by various fractional areas (dashed lines in Figure 15b) improves agreement with the observed distribution to some degree, although the weaker overall H_2O versus temperature correlations in the NA monsoon makes a quantitative link to theory less

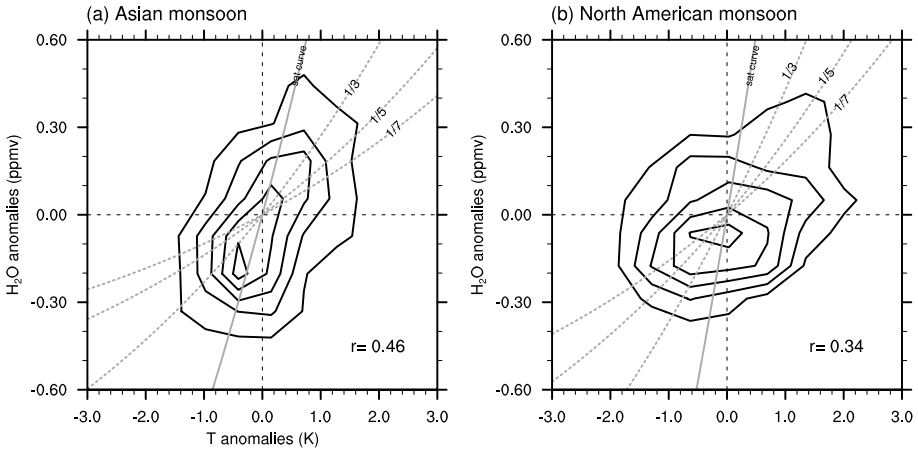

Figure 15. The contours indicate the two-dimensional distribution of 100 hPa water vapor anomalies versus 100 hPa temperature in the subtropics for the (a) Asian monsoon and (b) NA monsoon (specific areas are noted in the text). The contours enclose 90% (outer contour), 70, 50, 30, and 10% of all of the daily data points during June to August 2005–2013. Time series were smoothed with a 3 day running average, and water vapor anomalies are lagged by 6 days with respect to the temperatures, which maximizes the overall correlations. In each panel the solid grey line indicates the relationship expected from dehydration at 100% relative humidity according to Clausius-Clapeyron, and the dashed lines indicate the results from an idealized calculation where the dehydrated air is diluted into the wider monsoon region (the fractions on the dashed lines indicate the fractional area of the two regions, as discussed in text).

compelling than for the Asian monsoon. Part of the differences with the Asian monsoon may result from the much weaker circulation and isolating influence of the NA monsoon, so that subtropical dehydration is effectively more diluted, producing weaker overall correlations.

4. Summary and Discussion

The Asian and NA monsoon regions have a dominant influence on LS water vapor during NH summer, and transport from these regions likely influence the global stratosphere [e.g., *Gettelman et al*., 2004; *Ploeger et al*., 2013]. The objective of this study is to examine the natural (subseasonal) variations of water vapor in the monsoon regions and their links to deep convection and large-scale temperatures and circulation, to understand processes that maintain the climatological behavior.

Time series of LS water vapor in the monsoon regions show large subseasonal fluctuations, in addition to significant year-to-year variability (Figure 4). The nature of the year-to-year changes is not well understood. Based on previous work linking stratospheric water vapor with QBO and ENSO influences [e.g., *Geller et al*., 2002; *Gettelman et al*., 2001] we have modeled the interannual variations in the monsoon regions based on regressions onto standard QBO and ENSO indices. These regressions indeed capture some components of interannual variability, although we emphasize that the physical links to the QBO and ENSO are poorly understood, and this is simply an empirical method to remove some components of interannual variability. As a note, the predominant variability in the monsoon regions is on subseasonal time scales (as seen in Figure 4), and our composite results (and overall conclusions) are not changed if we choose a different method or do not remove the interannual variability. The subseasonal variability in LS water vapor is significantly higher over Asia as compared to the NA monsoon, and this may be related to the significantly stronger deep convection and circulation for the Asian monsoon or to the more confined behavior of the Asian anticyclone.

Composited variations in the Asian monsoon show that dry LS water vapor anomalies are linked to relatively stronger deep convection over ~20–30°N and ~80–130°E, overlapping the region of strongest climatological deep convection near 80–110°E (Figure 5a). There is corresponding reduced convection to the west, so that there is an east-west dipole structure to the fluctuations in deep convection. Variations in tropospheric column diabatic heating are closely related to OLR anomalies (cf. Figures 5b and 7). Nearly opposite patterns are found for composites of wet stratospheric anomalies. Variations in deep convection precede changes in LS water vapor by ~0–10 days, and time lag calculations (Figure 6) suggest oscillatory behavior in the system with time scale of 30–40 days (consistent with previous analyses of deep convection in the Asian monsoon [e.g., *Lau and Chan*, 1986]). This can directly result in 30–40 day variability in LS water vapor, as seen in Figure 10. Furthermore, the east-west dipole patterns in convection linked to extreme LS water vapor (Figure 5) are similar to behavior identified for intraseasonal oscillations in the Asian monsoon region [e.g., *Lau and Chan*, 1986; *Kikuchi et al*., 2012]. These similarities in space-time behavior suggest that intraseasonal variations in LS water vapor are probably linked to the more well-known intraseasonal variability of the monsoon circulation, via modulation of temperatures in the subtropical lower stratosphere. We have tested correlations between monsoon average LS water vapor (Figure 4c) and established indices of the monsoon variability (such as the Boreal Summer Intraseasonal Oscillation indices of *Kikuchi et al*. [2012]), and find weak but significant correlations (~0.2), suggesting a physical link with large-scale monsoon circulation.

The link between enhanced deep convection and a relatively dry stratosphere (and vice versa) is surprising at first sight, as one might expect stronger convection to result in wet stratospheric anomalies (via effects of overshooting convection [e.g., *Dessler and Sherwood*, 2004]). However, the observed links are explained by the large-scale temperature variations that accompany the changes in convection: the enhanced convection in the troposphere is linked to cooling in the subtropical LS, which is the region of most relevance for dehydration in the monsoon region (as discussed in *Wright et al*. [2011]). These subtropical temperatures then directly influence dehydration in the monsoon region as a whole. Very similar, mirror-image patterns are observed for wet stratospheric composites (less convection and relatively warm subtropical LS temperatures). The LS subtropical temperatures are part of the large-scale temperature and circulation response to convection, including out-of-phase temperature variations between the troposphere and stratosphere, and balanced variations in the strength of the UTLS monsoon anticyclone. These changes modulate the climatological structure, with stronger anticyclonic circulation for enhanced deep convection. For both wet and dry

anomalies in LS water vapor, variations in deep convection (and diabatic heating) within the monsoon system precede and force the dynamic variability leading to the observed changes in the stratosphere.

Overall, similar behavior is observed for composites of NA monsoon water vapor, including dry H_2O anomalies tied to enhanced deep convection (Figure 11b) and cold subtropical LS temperatures (and mirror-image results for wet composites). Likewise, large-scale balanced variations in temperature and circulation occur for the NA monsoon region, although in this case the patterns are shifted slightly northward from the climatological anticyclone, and the largest-temperature anomalies occur over ~30–40°N. This behavior may result from the fact that the anomalies in deep convection occur over ~20–35°N (Figure 11), north of the climatological maximum near Central America (~0–15°N) (i.e., both the OLR and dynamical responses are shifted northward from their climatological maxima). In any case, the overall similarity to variability within the Asian monsoon is clear, especially the subtropical LS temperature changes that are coupled to monsoon water vapor. While *Higgins and Shi* [2000] present evidence for coherent low-frequency (30–60 day) variations of the NA monsoon, our results do not show a strong influence for such variability.

The mechanism of large-scale dehydration controlling LS monsoon water vapor is consistent with calculations comparing observed water vapor-temperature changes with expectations from simple theory (dehydration at 100% relative humidity following Clausius-Clapeyron scaling), taking into account dilution of the dehydrated air into the larger monsoon region. The water vapor-temperature relationship exhibits significant correlation for the Asian monsoon (Figure 15a), where the variability in water vapor is relatively large and the strong circulation contributes to confined air masses. Assuming that dilution approximately scales as the area of the strongest subtropical temperature anomalies (boxed regions in Figure 8) to the wider monsoon regions (Figure 2), reasonable agreement is found between theory and the observed statistics (Figure 15a). This supports the interpretation that subtropical temperatures primarily control LS summer monsoon water vapor. In comparison, there is weaker correlation for the statistics over NA (although still statistically significant), and the observed H_2O versus temperature relationships (Figure 15b) suggest more dilution (consistent with less confinement in the weaker NA anticyclone).

We note that our calculations do not address the issue of the origin of enhanced LS water vapor in the monsoon regions. Because of the very strong background gradient in water vapor, transport of wet air to the LS can occur in broad-scale upward circulations [e.g., *Park et al*., 2007] and/or extreme deep convection. But the model calculations of *Wright et al*. [2011], in addition to the results shown here, suggest that in situ dehydration in the cold subtropics (along with confinement within the anticyclonic circulation) is the key process for maintaining the relatively wet air in the LS monsoon regions.

Our overall results demonstrate that variations in large-scale temperature, forced by deep convection, are the main controlling factor influencing LS water vapor on subseasonal time scales in the monsoon regions. The key temperatures occur in the subtropical LS, on the cold side of the anticyclonic circulation, as suggested by the model calculations of *Wright et al*. [2011]. These results are also consistent with the trajectory calculations of *Schoeberl et al*. [2013], who find relative occurrence maxima in "final dehydration" points in the subtropical monsoon regions during NH summer (consistent with the boxed regions highlighted here in Figures 8 and 13). Our results support the surprising conclusion that enhanced deep convection in the monsoon regions leads to colder subtropical temperatures and lower stratospheric water vapor, which is opposite of the result expected if direct injection from overshooting convection was the controlling process. *Anderson et al*. [2012] propose that enhanced deep convection in a changing climate could lead to higher amounts of water vapor in the monsoon regions, but our results suggest that stronger convection may produce the opposite effect on large scales.

Acknowledgments

We are grateful to Andy Dessler, Andrew Gettelman, Eric Jensen, George Kiladis, Joowan Kim, Laura Pan, and Mijeong Park for their comments and suggestions which have significantly improved the paper. Three anonymous referees provided constructive reviews which helped clarify and improve the manuscript. Tao Wang generously supplied access to the ERA-Interim heating rate data. The MLS water vapor data were obtained from http://mls.jpl.nasa.gov/products/h2o_product.php and the gridded OLR data from http://www.cdc.noaa.gov/. The ERA-Interim data were downloaded from http://apps.ecmwf.int/datasets/data/interim-full-daily/. This work was partially supported under the NASA Aura Science Program. The National Center for Atmospheric Research is operated by the University Corporation for Atmospheric Research, under sponsorship of the National Science Foundation.

References

Anderson, J. G., D. M. Wilmouth, J. B. Smith, and D. S. Sayres (2012), UV dosage levels in summer: Increased risk of ozone loss from convectively injected water vapor, *Science*, *337*(6096), 835–839, doi:10.1126/science.1222978.

Annamalai, H., and J. M. Slingo (2001), Active/break cycles: Diagnosis of the intraseasonal variability of the Asian summer monsoon, *Clim. Dyn.*, *18*, 85–102.

Bannister, R. N., A. O'Neill, A. R. Gregory, and K. M. Nissen (2004), The role of the South-East Asian monsoon and other seasonal features in creating the "tape recorder" signal in the unified model, *Q. J. R. Meteorol. Soc.*, *130*, 1531–1554, doi:10.1256/qj.03.106.

Dee, D. P., et al. (2011), The ERA-Interim reanalysis: Configuration and performance of the data assimilation system, *Q. J. R. Meteorol. Soc.*, *137*(656), 553–597.

Dessler, A. E., and S. C. Sherwood (2004), Effect of convection on the summertime extratropical lower stratosphere, *J. Geophys. Res.*, *109*, D23301, doi:10.1029/2004JD005209.
Dethof, A., A. O'Neill, J. M. Slingo, and H. G. J. Smit (1999), A mechanism for moistening the lower stratosphere involving the Asian summer monsoon, *Q. J. R. Meteorol. Soc.*, *125*, 1079–1106.
Devasthale, A., and S. Fueglistaler (2010), A climatological perspective of deep convection penetrating the TTL during the Indian summer monsoon from the AVHRR and MODIS instruments, *Atmos. Chem. Phys.*, *10*, 4573–4582.
Fu, R., et al. (2006), Convective transport over the Tibetan Plateau—A short-circuit of water vapor and polluted air to the global stratosphere, *Proc. Natl. Acad. Sci. U.S.A.*, *103*, 5664–5669, doi:10.1073/pnas.0601584103.
Fueglistaler, S., and P. H. Haynes (2005), Control of interannual and longer-term variability of stratospheric water vapor, *J. Geophys. Res.*, *110*, D24108, doi:10.1029/2005JD006019.
Geller, M. A., X. Zhou, and M. Zhang (2002), Simulations of the interannual variability of stratospheric water vapor, *J. Atmos. Sci.*, *59*, 1076–1085.
Gettelman, A., W. J. Randel, S. Massie, F. Wu, W. G. Read, and J. M. Russell III (2001), El Niño as a natural experiment for studying the tropical tropopause region, *J. Clim.*, *14*, 3375–3392.
Gettelman, A., D. E. Kinnison, T. J. Dunkerton, and G. P. Brasseur (2004), Impact of monsoon circulations on the upper troposphere and lower stratosphere, *J. Geophys. Res.*, *109*, D22101, doi:10.1029/2004JD004878.
Giorgetta, M. A., and L. Bengtsson (1999), Potential role of the quasi-biennial oscillation in the stratosphere-troposphere exchange as found in water vapor in general circulation model experiments, *J. Geophys. Res.*, *104*, 6003–6019, doi:10.1029/1998JD200112.
Hanisco, T. F., et al. (2007), Observations of deep convective influence on stratospheric water vapor and its isotopic composition, *Geophys. Res. Lett.*, *34*, L04814, doi:10.1029/2006GL027899.
Higgins, R. W., and W. Shi (2000), Intercomparison of the principal modes of interannual and intraseasonal variability of the North American monsoon system, *J. Clim.*, *14*, 403–417.
Holton, J. R., and A. Gettelman (2001), Horizontal transport and dehydration in the stratosphere, *Geophys. Res. Lett.*, *28*, 2799–2802, doi:10.1029/2001GL013148.
Hoskins, B. J., and M. J. Rodwell (1995), A model of the Asian summer monsoon, I, The global scale, *J. Atmos. Sci.*, *52*, 1329–1340.
James, R., M. Bonazzola, B. Legras, K. Surbled, and S. Fueglistaler (2008), Water vapor transport and dehydration above convective outflow during Asian monsoon, *Geophys. Res. Lett.*, *35*, L20810, doi:10.1029/2008GL035441.
Kikuchi, K., B. Wang, and Y. Kajikawa (2012), Bimodal representation of the tropical intraseasonal oscillation, *Clim. Dyn.*, *38*, 1989–2000, doi:10.1007/s00382-011-1159-1.
Lau, K.-M., and P. H. Chan (1986), Aspects of the 40–50 day oscillation during northern summer as inferred from outgoing longwave radiation, *Mon. Weather Rev.*, *114*, 1354–1367.
Livesey, N., et al. (2011), EOS MLS version 3.3 level 2 data quality and description document, *Tech. Rep.*, Jet Propul. Lab., Calif. Inst. of Technol., Pasadena, Calif.
Milz, M., et al. (2005), Water vapor distributions measured with the Michelson Interferometer for Passive Atmospheric Sounding on board Envisat (MIPAS/Envisat), *J. Geophys. Res.*, *110*, D24307, doi:10.1029/2005JD005973.
Park, M., W. J. Randel, A. Gettelman, S. T. Massie, and J. H. Jiang (2007), Transport above the Asian summer monsoon anticyclone inferred from Aura Microwave Limb Sounder tracers, *J. Geophys. Res.*, *112*, D16309, doi:10.1029/2006JD008294.
Ploeger, F., et al. (2013), Horizontal water vapor transport in the lower stratosphere from subtropics to high latitudes during boreal summer, *J. Geophys. Res. Atmos.*, *118*, 8111–8127, doi:10.1002/jgrd.50636.
Randel, W. J., A. Gettelman, F. Wu, J. M. Russell III, J. Zawodny, and S. Oltmans (2001), Seasonal variation of water vapor in the lower stratosphere observed in Halogen Occultation Experiment data, *J. Geophys. Res.*, *106*, 14,313–14,325, doi:10.1029/2001JD900048.
Randel, W. J., R. R. Garcia, N. Calvo, and D. Marsh (2009), ENSO influence on zonal mean temperature and ozone in the tropical lower stratosphere, *Geophys. Res. Lett.*, *36*, L15822, doi:10.1029/2009GL039343.
Randel, W. J., E. Moyer, M. Park, E. Jensen, P. Bernath, K. Walker, and C. Boone (2012), Global variations of HDO and HDO/H_2O ratios in the UTLS derived from ACE-FTS satellite measurements, *J. Geophys. Res.*, *117*, D06303, doi:10.1029/2011JD016632.
Ray, E. A., et al. (2004), Evidence of the effect of summertime midlatitude convection on the subtropical lower stratosphere from CRYSTAL-FACE tracer measurements, *J. Geophys. Res.*, *109*, D18304, doi:10.1029/2004JD004655.
Rosenlof, K. H., A. F. Tuck, K. K. Kelly, J. M. Russell III, and M. P. McCormick (1997), Hemispheric asymmetries in water vapor and inferences about transport in the lower stratosphere, *J. Geophys. Res.*, *102*, 13,213–13,234, doi:10.1029/97JD00873.
Schoeberl, M. R., and A. E. Dessler (2011), Dehydration of the stratosphere, *Atmos. Chem. Phys.*, *11*, 8433–8446, doi:10.5194/acp-11-8433-2011.
Schoeberl, M. R., A. E. Dessler, and T. Wang (2013), Modeling upper tropospheric and lower stratospheric water vapor anomalies, *Atmos. Chem. Phys.*, *13*, 7783–7793, doi:10.5194/acp-13-7783-2013.
Schwartz, M. J., B. Read, M. Santee, N. Livesey, L. Froidevaux, A. Lambert, and G. Manney (2013), Convectively injected water vapor in the North American summer lowermost stratosphere, *Geophys. Res. Lett.*, *40*, 2316–2321, doi:10.1002/grl.50421.
Wang, P. K. (2003), Moisture plumes above thunderstorm anvils and their contributions to cross-tropopause transport of water vapor in midlatitudes, *J. Geophys. Res.*, *108*(D6), 4194, doi:10.1029/2002JD002581.
Wright, J. S., R. Fu, S. Fueglistaler, Y. S. Liu, and Y. Zhang (2011), The influence of summertime convection over Southeast Asia on water vapor in the tropical stratosphere, *J. Geophys. Res.*, *116*, D12302, doi:10.1029/2010JD015416.
Yasunari, T. (1981), Structure of an Indian summer monsoon system with a period around 40 days, *J. Meteorol. Soc. Jpn.*, *59*, 336–354.